

01 Jan 2019

## Near-Field Electrospinning of a Polymer/Bioactive Glass Composite to Fabricate 3D Biomimetic Structures

Krishna C. R. Kolan

Jie Li


Sonya Roberts

Julie A. Semon

Missouri University of Science and Technology, [semonja@mst.edu](mailto:semonja@mst.edu)

*et. al.* For a complete list of authors, see [https://scholarsmine.mst.edu/biosci\\_facwork/297](https://scholarsmine.mst.edu/biosci_facwork/297)

Follow this and additional works at: [https://scholarsmine.mst.edu/biosci\\_facwork](https://scholarsmine.mst.edu/biosci_facwork)

 Part of the [Biology Commons](#), [Materials Science and Engineering Commons](#), and the [Mechanical Engineering Commons](#)

### Recommended Citation

K. C. Kolan et al., "Near-Field Electrospinning of a Polymer/Bioactive Glass Composite to Fabricate 3D Biomimetic Structures," *International Journal of Bioprinting*, vol. 5, no. 1, Whioce Publishing Pte. Ltd., Jan 2019.

The definitive version is available at <https://doi.org/10.18063/ijb.v5i1.163>



This work is licensed under a [Creative Commons Attribution 4.0 License](#).

This Article - Journal is brought to you for free and open access by Scholars' Mine. It has been accepted for inclusion in Biological Sciences Faculty Research & Creative Works by an authorized administrator of Scholars' Mine. This work is protected by U. S. Copyright Law. Unauthorized use including reproduction for redistribution requires the permission of the copyright holder. For more information, please contact [scholarsmine@mst.edu](mailto:scholarsmine@mst.edu).

## RESEARCH ARTICLE

# Near-field electrospinning of a polymer/bioactive glass composite to fabricate 3D biomimetic structures

Krishna C. R. Kolan<sup>1\*</sup>, Jie Li<sup>1</sup>, Sonya Roberts<sup>1</sup>, Julie A. Semon<sup>2</sup>, Jonghyun Park<sup>1</sup>, Delbert E. Day<sup>3</sup>, Ming C. Leu<sup>1</sup>

<sup>1</sup>Department of Mechanical and Aerospace Engineering, Missouri University of Science and Technology, Rolla, MO, USA

<sup>2</sup>Department of Biological Sciences, Missouri University of Science and Technology, Rolla, MO, USA

<sup>3</sup>Department of Materials Science and Engineering, Missouri University of Science and Technology, Rolla, MO, USA

**Abstract:** Bioactive glasses have recently gained attention in tissue engineering and three-dimensional (3D) bioprinting because of their ability to enhance angiogenesis. Some challenges for developing biological tissues with bioactive glasses include incorporation of glass particles and achieving a 3D architecture mimicking natural tissues. In this study, we investigate the fabrication of scaffolds with a polymer/bioactive glass composite using near-field electrospinning (NFES). An overall controlled 3D scaffold with pores, containing random fibers, is created and aimed to provide superior cell proliferation. Highly angiogenic borate bioactive glass (13-93B3) in 20 wt.% is added to polycaprolactone (PCL) to fabricate scaffolds using the NFES technique. Scaffolds measuring 5 mm × 5 mm × 0.2 mm<sup>3</sup> in overall dimensions were seeded with human adipose-derived mesenchymal stem cells to investigate the cell viability. The cell viability on PCL and PCL+glass scaffolds fabricated using NFES technique and 3D printing is compared and discussed. The results indicated higher cell proliferation on 3D biomimetic scaffolds fabricated by NFES technique.

**Keywords:** Near-field electrospinning; three-dimensional biomimetic scaffold; polycaprolactone; polymer/bioactive glass composite; borate bioactive glass; human adipose-derived stem cells

\*Correspondence to: Krishna C. R. Kolan, Department of Mechanical and Aerospace Engineering, Missouri University of Science and Technology, Rolla, MO, USA; kolank@mst.edu

**Received:** October 1, 2018; **Accepted:** October 8, 2018; **Published Online:** December 21, 2018

**Citation:** Kolan KCR, Li J, Roberts S, *et al.*, 2019, Near-field electrospinning of a polymer/bioactive glass composite to fabricate 3D biomimetic structures. *Int J Bioprint*, 5(1): 163. <http://dx.doi.org/10.18063/ijb.v5i1.163>

## 1. Introduction

Porosity, pore geometry, and pore size distribution are the most important parameters in scaffold fabrication in the field of tissue engineering. Different cell types require different pore sizes for optimal growth and proliferation<sup>[1]</sup>. Previous investigations have shown that pore geometry in three-dimensional (3D) scaffolds mimicking natural tissue architecture could offer a superior environment for cell proliferation<sup>[2]</sup>. While powder or resin bed-based additive manufacturing (AM) techniques offer flexibility to fabricate scaffolds mimicking natural tissue architecture, fabricating scaffolds with complex pore

geometries are limited with extrusion-based 3D printing methods<sup>[3-5]</sup>. Extrusion-based 3D printing is the most versatile and widely adopted AM technique in bioprinting because of a wide range of hydrogels that are suitable for cell suspension and extrusion<sup>[6]</sup>. However, creating macrostructures that mimic natural tissue architecture with extrusion 3D printing has been a challenge.

On the other hand, electrospinning is a mature technology for fabricating aligned and randomly oriented fiber mats for different tissue engineering applications<sup>[7]</sup>. In recent years, a most common approach adopted by researchers to achieve the 3D biomimetic structures has

been to combine the electrospinning and 3D printing techniques to provide a nanofiber mesh in between the 3D printed macroporous layers<sup>[8]</sup>. An alternative approach to the traditional electrospinning is called near-field electrospinning (NFES), where the substrate distance from nozzle tip is decreased to control the fiber deposition<sup>[9,10]</sup>. In NFES technique, fiber instability is restricted because of the shorter substrate distance and deposition is precisely controlled to obtain the desired part shape. Figure 1 illustrates the type of fiber deposition obtained at different substrate distances. In this work, the substrate distance was maintained such that the fabricated scaffold would have an overall defined shape with directional filaments. Simultaneously, it was also made sure that the deposited fibers would have a certain degree of randomness to create the biomimetic architecture that resembles the cancellous bone.

Researchers have investigated electrospinning of polycaprolactone (PCL) + glass composites (typically, 5–10 wt.% silicate-based glass) to improve the scaffold bioactivity<sup>[11,12]</sup>. In this study, we use borate glass (13-93B3 or B3) that is biocompatible, osteoconductive, and angiogenic and has a higher reaction rate (5–10 times faster than silicate glasses) and is antimicrobial<sup>[13]</sup>. The glass can heal even difficult-to-heal wounds by generating a healthy scar-free tissue with improved vascularization. In the current work, we investigate the feasibility of fabricating a bioactive 3D scaffold mimicking the native bone architecture using NFES of PCL+B3 glass composite.

## 2. Materials and Methods

### 2.1. Preparation of PCL+B3 Glass Paste

0.25 g of B3 glass (Mo-Sci Corporation, Rolla, MO) particles of  $< \sim 20 \mu\text{m}$  were ultrasonicated for 2 min in 3 ml chloroform (CF) (Sigma-Aldrich, St. Louis, MO). B3 glass composition can be found in literature<sup>[14]</sup>, 1 g of PCL (Polysciences, Warrington, PA; M.W. = 50,000 g/mol) was added immediately after

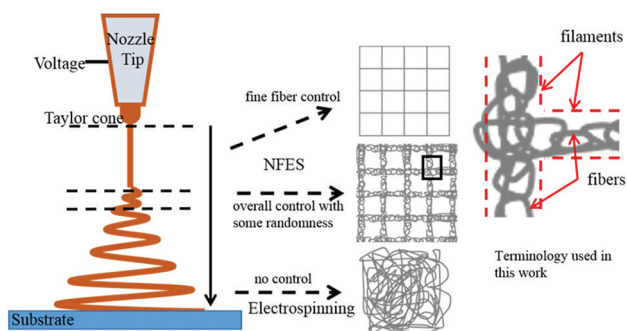


**Figure 1.** Illustration of the fiber and filament control with increasing substrate distance from nozzle tip during electrospinning.

ultrasonication and materials were uniformly mixed for 5 min at 2000 RPM in a planetary mixer (SpeedMixer™, FlakTek Inc., Landrum, SC). The weight ratio of materials was selected in such a way to provide a 20% glass in weight in the fabricated composite scaffolds after eventual CF evaporation.

### 2.2. Scaffold Fabrication and Characterization

For NFES, a home-built, three-axis gantry system with pressurized air extrusion and a power source was utilized. Scaffolds were fabricated on an aluminum foil placed on a metal substrate and a custom-made software interface was used to control the printing parameters including applied voltage, air pressure, and printing speed. A metal tip (0.25 mm internal diameter) was used to fabricate scaffolds measuring  $20 \text{ mm} \times 20 \text{ mm} \times 0.2 \text{ mm}^3$ , which were later cut into  $(5 \text{ mm} \times 5 \text{ cm} \times 0.2 \text{ mm}^3)$  dimensions for *in vitro* assessment. For comparison, scaffolds were also 3D printed using the same paste composition as described in our previous work<sup>[14]</sup>. Optical microscopic images were used to measure the filament width and pore sizes with at least 10 measurements and the results were reported as average  $\pm$  standard deviation. Scaffolds were soaked in 2 ml of the complete culture media (CCM) to simulate the *in vitro* conditions and evaluate the surface morphology and formation of hydroxyapatite-like material on the surface. After soaking for up to 7 days in CCM, scaffolds were dried overnight, coated with Au-Pd, and observed under a scanning electron microscope (S-4700, Hitachi, Japan).

### 2.3. Cell Culture

Frozen vials of approximately  $1 \times 10^6$  adipose-derived human mesenchymal stem cells (ASCs) were obtained from three separate donors (LaCell, New Orleans, LA). Vials were thawed, plated on 150 cm<sup>2</sup> culture dishes (Nunc, Rochester, NY) in 25 mL CCM consisting of 10% fetal bovine serum (FBS, Corning, Manassas, VA), alpha-minimum essential media ( $\alpha$ -MEM, Sigma-Aldrich, St. Louis, MO), 1%  $\times 100$  L-glutamine (GE Life Sciences, Logan, UT), 1%  $\times 100$  antibiotic/antimycotic (GE Life Sciences, Logan, UT), and incubated at 37.5°C with 5% humidified CO<sub>2</sub>. After 24 h, the media were removed and adherent, viable cells were washed twice with phosphate-buffered saline (PBS), harvested with 0.25% trypsin/1 mM ethylenediaminetetraacetic acid (Gibco), and replated at 100 cells/cm<sup>2</sup> in CCM. Media were changed every 3–4 days. Subconfluent cells ( $\leq 70\%$  confluent) between passage 2 and passage 6 were used for all experiments as subsequent passages could affect pluripotent properties of ASCs.

### 2.4. Cell Viability

Scaffolds were seeded with 30,000 ASCs suspended in 30  $\mu\text{l}$  of CCM. After a 2 h incubation to allow cell

attachment, scaffolds were transferred to 35 mm Petri dishes with 2 ml of CCM. A Live/Dead cell imaging kit (ref. R37601, Eugene, OR) was used for qualitative assessment of cell viability. Briefly, after a 24 h incubation period, scaffolds were washed with PBS, stained for 30 min at room temperature, and examined under a fluorescent microscope (Olympus IX51, Melville, NY). Five scaffolds were examined per experimental group, with at least five pictures taken per scaffold.

To quantify cell viability, scaffolds were analyzed for total DNA using CyQuant cell proliferation assay (Invitrogen), using the manufacturer's protocol to normalize all results to cell number. Briefly, 24 h after seeding cells, cellularized scaffolds were gently washed with PBS and frozen at  $-80^{\circ}\text{C}$  overnight. Scaffolds were thawed the next day and analyzed with CyQuant. A sample size of  $n = 5$  was used for all experiments except for CyQuant assay for 3D printed PCL scaffolds ( $n = 4$ ). Scaffolds without cells were used for background controls. One-way ANOVA was performed in Minitab to analyze the results and difference was considered significant if  $P < 0.05$ .

### 3. Results and Discussion

#### 3.1. Scaffold Fabrication

The effect of fabrication parameters including applied electric field, printing speed, and extrusion pressure on the filament deposition was investigated. The above parameters control the porosity of the fabricated part by changing the filament size, fiber size, and the amount of deposited material as shown in Figure 2a. The filament and fiber sizes at different parameters are shown in Table 1. A 10 kV/cm electric field with 5 mm/s printing speed and 30 psi extrusion pressure (test #8) provided a suitable filament with randomly distributed small fibers to create a biomimetic 3D structure. The printing schema and fabricated 3D scaffold with cancellous bone microstructure similarities can be observed in Figures 2f and 2g. Furthermore, the pore size distribution in NFES scaffolds varied from 20  $\mu\text{m}$  to 250  $\mu\text{m}$  that are desirable for bone tissue growth.

In this study, one of our aims was also to compare and contrast the NFES scaffolds with 3D printing scaffolds in terms of bioactivity and cell proliferation. Therefore, we have used the solvent-based 3D printing process to fabricate scaffolds with the same compositions of PCL+B3 glass and PCL pastes used in NFES technique. More details about the solvent-based 3D printing and scaffold fabrication with PCL+B3 glass composite (up to 50 wt.% glass) can be found in our previous work<sup>[14,15]</sup>. 3D printed scaffolds were designed to have pore sizes not exceeding the pore sizes obtained using NFES technique (i.e., 250  $\mu\text{m}$ ) and to reflect an average pore size. A printing speed of 20 mm/s, air pressure of 30 psi, and filament-to-filament spacing of 0.35 mm were used to fabricate the scaffold. The average filament width of  $167 \pm 38 \mu\text{m}$  and pore size of  $188 \pm 28 \mu\text{m}$  were obtained for the 3D printed scaffold.

#### 3.2. Scaffold Bioactivity

The scaffold porosity was calculated based on 2D optical images after the printing of the first two layers of the scaffold with both processes. The obtained porosity for NFES scaffold was ~50% compared to ~30% for 3D printed scaffold. The higher porosity and wide range of pore sizes of NFES scaffold are beneficial for B3 glass dissolution because of the larger surface area. Scaffolds were soaked in CCM for up to 7 days to evaluate the formation of hydroxyapatite (HA)-like layer on the scaffold surface (Figure 3). The results indicated nanosized HA-like crystal formations on scaffolds made by both processes. The crystals were uniformly spread out on NFES scaffold surface and were observed in patches on 3D printed scaffolds. This indicates a faster B3 glass dissolution from NFES scaffolds compared to 3D printed scaffolds. The X-ray diffraction results showed peaks indicating the formation of non-stoichiometric HA which is consistent with our previous studies where PCL+B3 glass scaffolds showed similar conversion<sup>[14]</sup>.

#### 3.3. Cell Viability and Proliferation

Viability of ASCs was studied by seeding cells on scaffolds and performing live/dead assay after 1 day and

**Table 1.** Effects of fabrication parameter on filament and fiber sizes in NFES

Test	Electric field (kV/cm)	Printing speed (mm/s)	Extrusion pressure (psi)	Filament size ( $\mu\text{m}$ )	Fiber size ( $\mu\text{m}$ )
#1	12	7.5	50	$565 \pm 37.4$	$80.2 \pm 12.1$
#2	10	7.5	50	$567.5 \pm 37.9$	$46.8 \pm 6.9$
#3	8	7.5	50	$562.5 \pm 52.6$	$87.2 \pm 20.8$
#4	6	7.5	50	N/A	$103 \pm 10.9$
#5	10	5	50	$578.75 \pm 41.9$	$47.8 \pm 18.5$
#6	10	2.5	50	$501 \pm 28.6$	$99.8 \pm 28.8$
#7	10	5	40	$350.25 \pm 87.2$	$42.2 \pm 18.5$
#8	10	5	30	$517.5 \pm 27.9$	$33.4 \pm 6.3$
#9	10	5	20	N/A	$48 \pm 12.0$



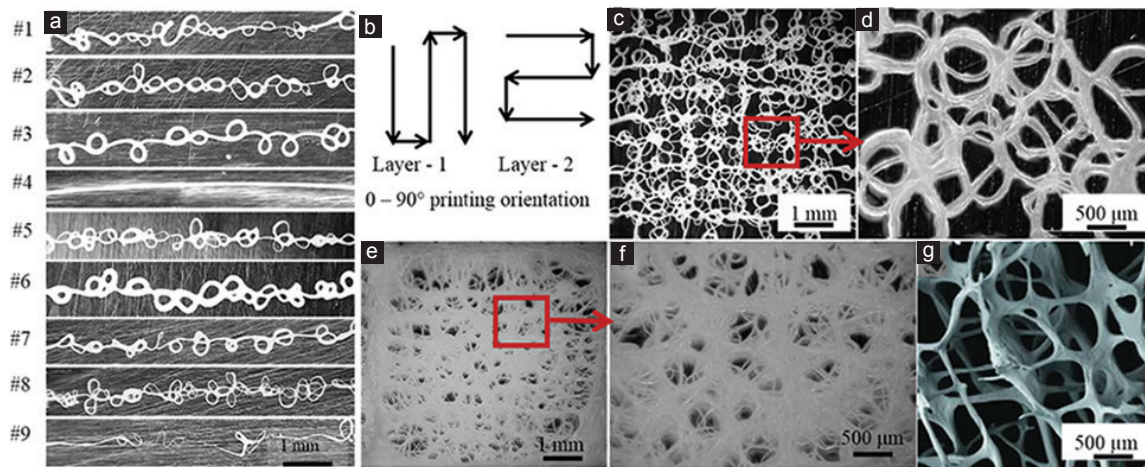


**Figure 2.** Near-field electrospinning of polycaprolactone (NFES) +B3 glass composite. (a) Fiber deposition control with different NFES fabrication parameters, (b) printing schema, (c) after printing one raster in both 0° and 90° orientation, (d) magnified image showing the fiber dimensions, (e) 10-layer scaffold, (f) magnified image of the 10-layer scaffold, and (g) cancellous bone microstructure (reproduced with permission<sup>[16]</sup>).

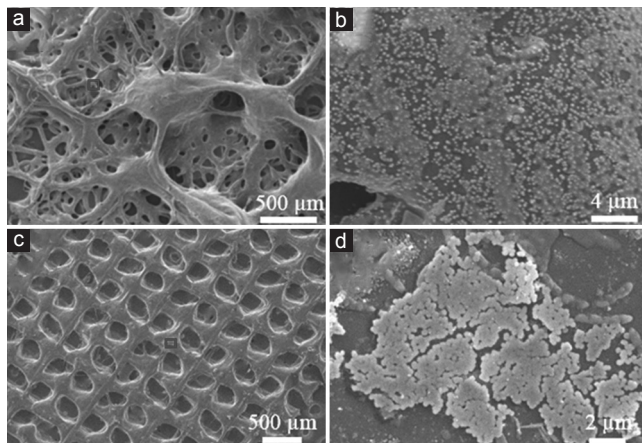


**Figure 3.** Scanning electron microscope images of near-field electrospinning of polycaprolactone (NFES) and three-dimensional (3D) printed scaffolds soaked in complete culture media for 7 days. Scaffolds showed HA-like crystal formations on the scaffold surface. (a-b) NFES scaffold and its magnified image, (c-d) 3D printed scaffold and its magnified image.

7 days. The assay reagents consist of a non-fluorescent calcein dye which is converted to green fluorescent calcein after intracellular esterases in live cells causing the live cells to stain green. In dying or dead cells, a bright red fluorescence is generated on binding to DNA. Overall, in all scaffold types, the results indicated more live cells in comparison to dead cells (Figure 4). Specifically, more live cells were observed in all NFES scaffolds with or without glass in comparison to 3D printed scaffolds after 7 days incubation. This can be clearly seen in Figures 4g-h. However, the live/dead assay images were not used to quantify the cell viability results because of the high background staining of B3 glass particles, which

can be observed in PCL + B3 glass composite scaffolds (Figures 4b-f and 4d-h). In normal conditions, the non-fluorescent calcein acetoxymethyl compound present in live/dead assay transports into cells, and intracellular esterases remove the acetoxymethyl group, thereby producing strong green fluorescence. It is believed that the borate ions present in the B3 glass interfere with the acetoxymethyl group, thereby producing strong green fluorescence even without cells. The PCL only scaffolds do not exhibit strong fluorescence in the absence of glass particles, which can be clearly observed in Figures 4a-e and 4c-g (strong green fluorescence in Figure 4g is because of more cells and not material). The background staining makes it difficult to contrast and quantify cells on PCL+B3 glass scaffolds using the ImageJ software. The green fluorescence and staining of the 3D printed PCL+B3 glass scaffold filament can be clearly observed in Figures 4b-f. Overall, the live/dead assay results qualitatively indicated more cell ASC proliferation in NFES scaffolds compared to 3D printed scaffolds.

To quantify cell proliferation, CyQuant assay was performed on the ASC-seeded scaffolds (Figure 5). The CyQuant GR is a green fluorescence dye that intensifies after it binds to the nucleic acid of DNA to provide a reading that is then converted to cell number based on the standard curve. The results indicated increased cell proliferation in NFES PCL scaffolds compared to 3D printed PCL scaffolds after 1 day and 7 days incubation. However, the results are not statistically significant with  $P = 0.4$ . A wide pore size distribution in NFES scaffolds could have provided uniform cell distribution and proliferation, whereas cells were mainly observed on filaments in 3D printed scaffolds. The Live/Dead

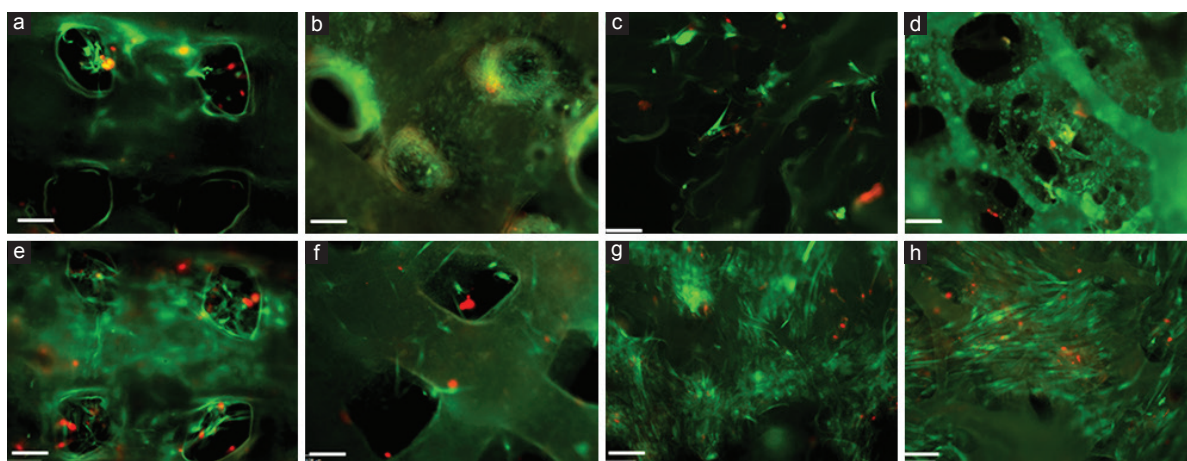


**Figure 4.** Live/dead images showing the viability of adipose-derived human mesenchymal stem cells seeded on scaffolds (scale bar: 100  $\mu$ m). (a-d) after 1 day and (e-h) after 7-day incubation, (a and e) three-dimensional (3D) printed polycaprolactone (PCL), (b and f) 3D printed PCL+B3 glass, (c and g) near-field electrospinning of polycaprolactone (NFES) PCL, (d and h) NFES PCL+B3 glass. NFES scaffolds show high cell proliferation after 7 days compared to 3D printed scaffolds

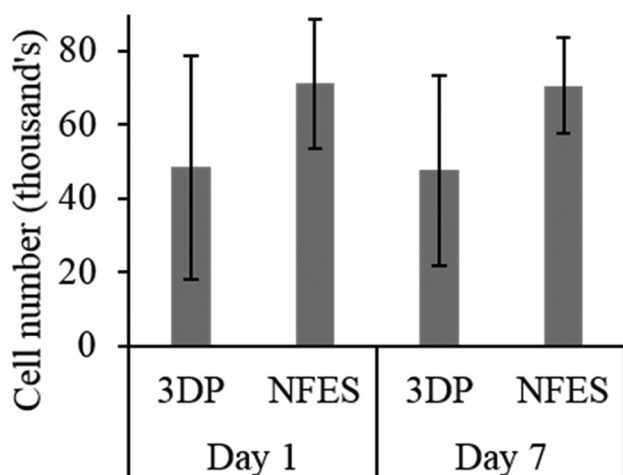


**Figure 5.** Cell proliferation measured by CyQuant. Near-field electrospinning of polycaprolactone scaffolds showed increased cell proliferation in polycaprolactone scaffolds. All scaffolds were seeded with 30,000 adipose-derived human mesenchymal stem cells

assay results consistently showed more number of cells in NFES scaffolds, and the CyQuant results are in consistent for PCL scaffolds as shown in Figure 5. In addition, more dead cells (red spots) were observed in PCL+B3 scaffolds (both NFES and 3D printed) compared to PCL only scaffolds (e.g., Figure 4g vs. 4h). One possible reason for a relatively higher cell death in PCL+B3 glass scaffolds compared to PCL only scaffolds could be because of the pH change due to B3 glass dissolution and the released ionic products which could harm cells, especially, in static culture conditions. Poor cell viability was previously reported on cell-seeded B3 glass scaffolds in static conditions that improved under dynamic conditions<sup>[2,17]</sup>. Regardless, with respect to PCL

only scaffolds, the *in vitro* assessment performed in this study definitively indicates improved ASC proliferation on NFES scaffolds in comparison to 3D printed scaffolds showing the potential of the NFES technique and significance of the biomimetic 3D structure compared to the 3D printed lattice structure. The additional advantage of NFES technique is that the process can be easily integrated for bioprinting applications with simultaneous bio-ink extrusion in a 3D architecture mimicking the extracellular matrix.

#### 4. Conclusion

This study investigated the feasibility of fabricating a biomimetic 3D scaffold with PCL and PCL/bioactive glass composite (20 wt.% glass) using the NFES technique. NFES scaffolds had a microstructure similar to the cancellous bone, ~50% porosity, and a wide pore distribution (20–250  $\mu$ m). In comparison with 3D printed scaffolds, NFES scaffolds were highly bioactive providing a faster glass dissolution and more uniform formation of hydroxyapatite-like crystalline formations throughout the scaffold surface after 7 days. Live/dead assessment with human adipose-derived mesenchymal stem cells indicated high cell proliferation and uniform cell distribution in NFES scaffolds compared to 3D printed scaffolds. Overall, the NFES technique showed the process potential for tissue engineering and bioprinting applications.

#### Acknowledgment

This research is funded by the Intelligent Systems Center and the Center for Biomedical Research at the Missouri University of Science and Technology. The glass used in this study was provided by MO-SCI Corporation, Rolla,

MO. The authors thank Bradley Bromet for his assistance during imaging.

## Conflicts of Interest and Funding

No conflicts of interest were reported by the authors.

## References

1. Bružauskaitė I, Bironaitė D, Bagdonas E, Bernotienė E. Scaffolds and cells for tissue regeneration: Different scaffold pore sizes-different cell effects. *Cytotechnology* 2016;68:355-69.
2. Kolan KC, Thomas A, Leu MC, Hilmas GE. *In vitro* assessment of laser sintered bioactive glass scaffolds with different pore geometries. *Rapid Prototyp J* 2015;21:152-8.
3. Kolan KC, Leu MC, Hilmas GE, Velez M. Effect of Architecture and Porosity on Mechanical Properties of Borate Glass Scaffolds Made by Selective Laser Sintering. 24<sup>th</sup> International. SFF symposium. An Additive Manufacturing Conference; 2013. p. 816-26.
4. Melchels FP, Barradas A M C, Van Blitterswijk C, de Boer J, Feijen J, Grijpma DW. Effects of the architecture of tissue engineering scaffolds on cell seeding and culturing. *Acta Biomater* 2010;6:4208-17.
5. Fu Q, Saiz E, Tomsia AP. Direct ink writing of highly porous and strong glass scaffolds for load-bearing bone defects repair and regeneration. *Acta Biomater* 2011;7:3547-54.
6. Ozbolat IT, Hospodiuk M. Current advances and future perspectives in extrusion-based bioprinting. *Biomaterials* 2016;76:321-43.
7. Li Y, Bou, Akl T, 2016, *Electrospinning in Tissue Engineering*, Electrospinning, Sajjad Haider and Adnan Haider, Intech Open. Available from: <<https://www.intechopen.com/books/electrospinning-material-techniques-and-biomedical-applications/electrospinning-in-tissue-engineering>>. [http://doi: 10.5772/65836](http://doi:10.5772/65836).
8. Giannitelli SM, Mozetic P, Trombetta M, Rainer A. Combined additive manufacturing approaches in tissue engineering. *Acta Biomater* 2015;24:1-11.
9. Daoheng S, Chieh C, Sha L, Lin L. Near-field electrospinning. *Nano Lett* 2006;6:839-42.
10. He XX, Zheng J, Yu GF, You MH, Yu M, Ning X, *et al.* Near-field electrospinning: Progress and applications. *J Phys Chem C* 2017;121:8663-78.
11. Moura D, Souza M T, Liverani L, Rellae G, Luzab GM, Mano JE, *et al.* Development of a bioactive glass-polymer composite for wound healing applications. *Mater Sci Eng C* 2017;76:224-32.
12. Liverani L, Lacina J, Roether JA, Boccardi E, Manuela S, Schmuki P, *et al.* Incorporation of bioactive glass nanoparticles in electrospun PCL/chitosan fibers by using benign solvents. *Bioact Mater* 2018;3:55-63.
13. Rahaman MN, Day DE, Bal BS, Fu Q, Jung SB. Bioactive glass in tissue engineering. *Acta Biomater* 2011;7:2355-73.
14. Murphy C, Kolan K, Li W, Semon J, Day D, Leu M. 3D bioprinting of stem cells and polymer/bioactive glass composite scaffolds for tissue engineering. *Int J Bioprinting* 2017;3:54-64.
15. Kolan K, Liu Y, Baldrige J, Leu MC. Solvent based 3D Printing of biopolymer/bioactive glass composite and hydrogel for tissue engineering applications. *Procedia CIRP* 2017;65:38-43.
16. Boyde A. Improved digital SEM of cancellous bone: Scanning direction of detection, through focus for in-focus and sample orientation. *J Anat* 2003;202:183-94.
17. Jung S. Borate Based Bioactive Glass Scaffolds for Hard and Soft Tissue Engineering. Doctoral Dissertations; 2010. p. 2075.